Volume 20 | Number 42 | 14 November 2018 | Pages 6643–6846

CrystEngComm

rsc.li/crystengcomm

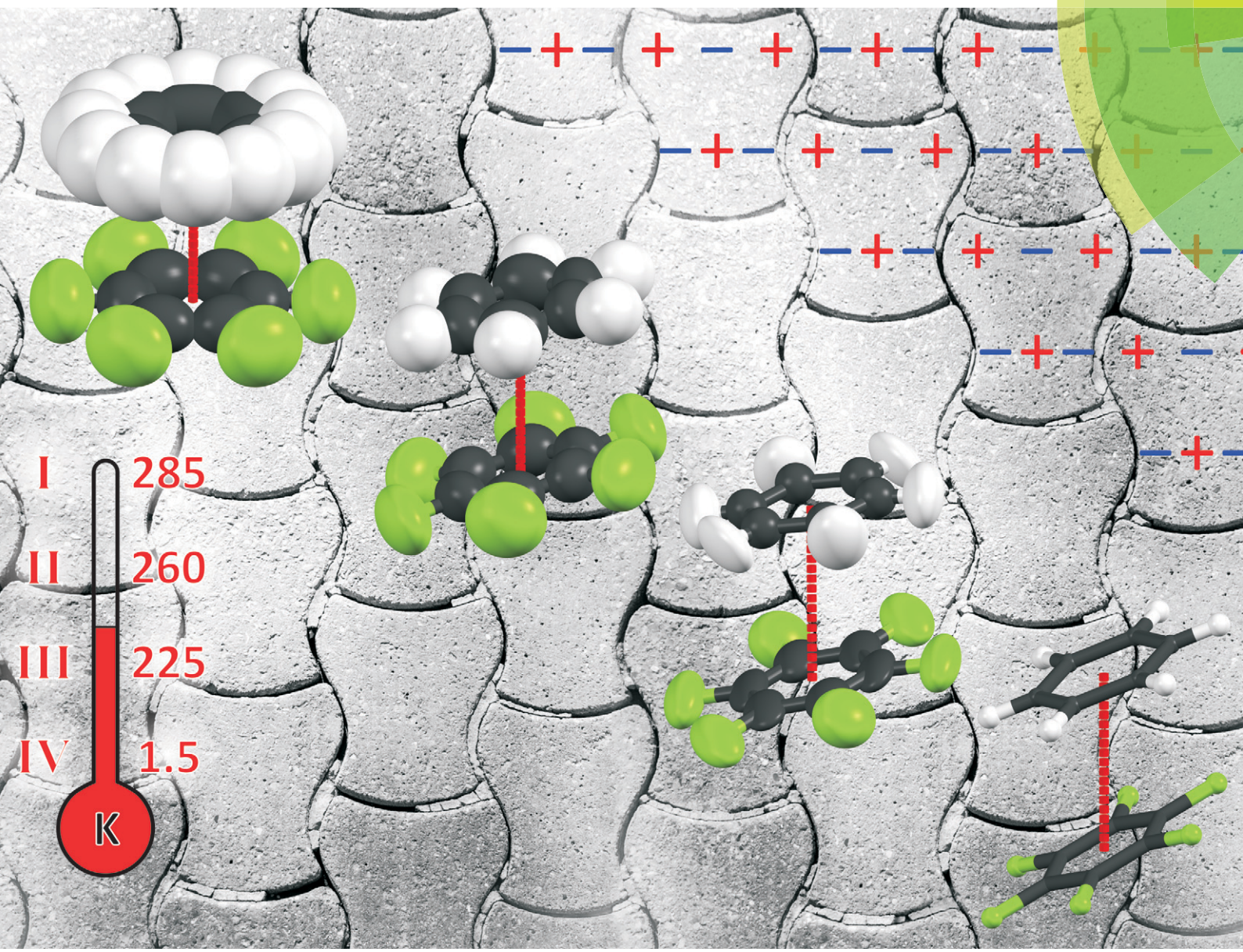

ROYAL SOCIETY OF CHEMISTRY

PAPER

Jeremy K. Cockcroft, Jeffrey H. Williams *et al.*

The temperature dependence of C–H···F–C interactions in benzene: hexafluorobenzene

CrystEngComm

PAPER

View Article Online
View Journal | View Issue

Cite this: *CrystEngComm*, 2018, **20**, 6677

The temperature dependence of C–H···F–C interactions in benzene : hexafluorobenzene†‡

Jeremy K. Cockcroft, *[a] Alexander Rosu-Finsen, [a] Andrew N. Fitch [b] and Jeffrey H. Williams*[c]

Received 18th July 2018,
Accepted 10th September 2018

DOI: 10.1039/c8ce01187g

rsc.li/crystengcomm

The evolution of the structure of the four solid phases of the prototype binary-adduct $C_6H_6:C_6F_6$ as a function of temperature has been investigated using X-ray and neutron diffraction. An explanation is proposed concerning changes in the arrangements of the molecules at each of the three phase transitions and the dynamics in $C_6H_6:C_6F_6$ are briefly compared with those of the adduct formed between mesitylene and C_6F_6. The observations are rationalised using simple models of intermolecular electrostatics.

Introduction

Understanding weak van der Waals interactions in solids is crucial for the prediction and control of organic structures.[1,2] Of particular interest to the community of crystal engineers is the design of organic co-crystals as alternatives to salts in the development of new materials in, *e.g.*, the pharmaceutical industry. For organic fluorine (*i.e.* covalently bonded as C–F), there is a general consensus that fluorine rarely forms hydrogen bonds[3,4] leading to questions about the nature of the interaction between neighbouring C–F and H–C bonds in the solid state, and as to whether or not such interactions can be used to design structures.[5,6] The need to understand this type of weak interaction has particular importance in the pharmaceutical sector, where a variety of fluorinated active pharmaceutical ingredients (API's) have been developed, *e.g.* for use as antidepressants (fluoxetine, the API in Prozac), as cholesterol lowering drugs (atorvastatin, the API in Lipitor), and as antibiotics (ciprofloxacin hydrochloride).[7]

One of the simplest organic co-crystals containing a molecule with many C–F bonds and without 'classical' hydrogen bonding is the 1:1 adduct of benzene (C_6H_6) and hexafluorobenzene (C_6F_6), first reported over 50 years ago.[8] Both C_6H_6 and C_6F_6 are liquids at room temperature, but the binary adduct is a solid under ambient conditions. The structure of the lowest temperature phase (IV) of this adduct was solved in 1991.[9] In addition to the complex with C_6H_6, C_6F_6 is known to form a series of 1:1 co-crystals with various methyl substituted benzenes including mesitylene (1,3,5-$C_6H_3Me_3$),[10,11] mellitene (C_6Me_6),[12,13] *p*-xylene (1,4-$C_6H_4Me_2$),[14] and durene (1,2,4,5-$C_6H_2Me_4$).[15] All these, and related co-crystals possess structural instabilities and contain (at least one) phase transition below their melting point.

One of the objectives of investigating such materials is to evaluate the role of C–H···F–C interactions in the crystal structures of solids formed from closely-packed columns, where each column is made of two alternating molecules. In particular, where the two alternating molecules are small aromatic molecules, but with different electron distributions, electron distributions cause the two species to 'bond' face-to-face through a weak electrostatic (electric quadrupole) interaction. The stacking interactions formed by C_6F_6 are of particular interest in this regard. Despite the earlier investigations by Dahl, and more recent studies (*e.g.* on substituted benzamides[16]), an understanding of the prototypical adduct material $C_6H_6:C_6F_6$ has proved intractable until now.

The type of weak, van der Waals intermolecular interactions seen in such solids are best described as: bond dipole–bond dipole interactions between the close-packed columns and quadrupole moment–quadrupole moment interactions within the columns. These are weak electrostatic interactions, which in crystals of organic molecules play a significant part in determining the structure of the solid when hydrogen bonding is absent. In addition, these interactions also determine the dynamics of the crystal architecture, *e.g.*, in initiating the various solid-state phase transitions seen in binary-adducts such as $C_6H_6:C_6F_6$ and 1,3,5-$C_6H_3Me_3:C_6F_6$,[11] which involve interactions between C–F bonds on one molecule in

[a] *Department of Chemistry, Christopher Ingold Laboratories, UCL, 20 Gordon Street, London WC1H 0AJ, UK. E-mail: j.k.cockcroft@ucl.ac.uk*
[b] *European Synchrotron Radiation Facility - 71, avenue des Martyrs, CS 40220, 38043 Grenoble Cedex 9, France*
[c] *Montpellier, France. E-mail: jeffreyhuw@hotmail.com*

† This paper is dedicated to Prof. Tor Dahl who pioneered the early structural studies on this class of adduct with some very elegant experiments.

‡ Electronic supplementary information (ESI) available: Additional experimental detail, crystallographic tables, and additional supporting figures are supplied. CIF files have been deposited at the Cambridge Crystallographic Data Centre with deposition numbers 1851535 (phase I), 1851536 (phase II), 1851537 (phase III), and 1851538 (phase IV). For ESI and crystallographic data in CIF or other electronic format see DOI: 10.1039/c8ce01187g

one of the columns and C–H bonds on molecules in an adjacent column. Consequently, these interactions give further stability, lateral or perpendicular to the axis of the closely packed columns. The lateral interactions are sometimes termed hydrogen bonds, but in fact, they are simple dipole–dipole interactions. However, as the molecules have no permanent electric-dipole moment, one must consider the asymmetry of the charge in the bonds of the molecules, *i.e.* one is considering a distributed multipole model of the attractive inter-column interactions. Whereas the attractive intra-column interactions can be considered as single-site multipole (quadrupole) interactions (referred to the centres-of-mass of the molecules). In benzene and hexafluorobenzene, the individual C–H and C–F bonds are polarized (the electronegativities of the atoms are very different) and the vector sum of the six bond dipoles is zero in both molecules. So therefore in C_6F_6, there are six $^{\delta+}C–F^{\delta-}$ bond dipoles disposed towards nearby $^{\delta-}C–H^{\delta+}$ bond dipoles in C_6H_6 molecules in adjacent columns.

The understanding of intermolecular interactions and cohesion in these binary adducts has changed over time. Originally, they were called 'charge-transfer solids'. It was thought that there was a donor–acceptor or π–π* bond between C_6H_6 and C_6F_6.[17–19] However, transfer of charge and the consequent molecular orbital changes are not supported by spectroscopy as the internal vibrations of the molecules in the adduct show only a small frequency shift when compared to those of the pure solids.[20,21]

An alternative model explaining structural cohesion in these adducts is provided by studies of their charge distribution.[22,23] Given the lack of an overall dipole moment in C_6H_6 and C_6F_6, the first non-vanishing electrical moment, which will dominate intermolecular interactions is the quadrupole moment. Experimental values of the quadrupole moment are available *via* the Buckingham technique of electric field-gradient induced birefringence.[24,25] For C_6H_6, the value of the quadrupole is large and negative: $-29.0 \pm 1.7 \times 10^{-40}$ C m^2, and for C_6F_6 the quadrupole moment is large and positive: $+31.7 \pm 1.7 \times 10^{-40}$ C m^2. The large negative value for C_6H_6, can be interpreted with the familiar picture of delocalized charge (π-cloud) above and below the plane of the C_6-ring. In contrast, due to the strong electronegativity of the fluorine atoms in C_6F_6, the electron charge density of the π-cloud is distorted towards the F atoms resulting in a larger component of electron density in the plane of the C_6-ring and, consequently, the sign of the quadrupole moment changes and is now large and positive. This makes C_6F_6 less susceptible to electrophilic attack than C_6H_6.

The ability to predict the solid-state packing of molecules, and to comprehend the observed molecular dynamics from knowledge of the electrical properties of the isolated molecules, is a goal that is much sought after. Although the strength of the various intermolecular interactions may be approximated, the problem is not straightforward. The utility of such modelling is the argument of this work.

Results and discussion

Powder neutron diffraction (PND) patterns collected on a sample of $C_6D_6:C_6F_6$ on the high-flux diffractometer D1B at the Institut Laue Langevin (ILL), Grenoble, are shown in Fig. 1 and S1.‡ The presence of three phase transitions on heating at 218, 255, and 281.5 K is immediately apparent. At the time of the measurements, the structures of these phases were unknown, and so only a limited interpretation of these results was possible.[26] However, it was apparent that significant hysteresis existed for the transition from phase III to phase IV, and that grinding a sample in liquid N_2 considerably reduces the amount of residual phase III in phase IV on cooling.

Powder neutron diffraction data were collected on a sample of $C_6D_6:C_6F_6$ on the high-resolution diffractometer D1A at the ILL and complementary synchrotron X-ray measurements on $C_6H_6:C_6F_6$ were made at the SRS, Daresbury, using beamline 2.3. Details of the experiments are to be found in the ESI‡ Sect. 2. At that time, the structure of phase IV was solved and possible unit cells were identified for the other three phases.[9] The comparative cell parameters given in Table 1 are based on recent Rietveld refinement to the original neutron data using structures determined recently (see ESI‡).

To take advantage of modern developments in hardware and software, a reinvestigation of $C_6H_6:C_6F_6$ was begun. Initially, the system was studied by variable temperature laboratory PXRD, but the combination of small capillary samples and hysteresis failed to provide sufficient insight to permit a determination of the structure of the unknown phases. Consequently, DSC measurements (ESI‡ Sect. 3) were made to better understand the nature of the phase transitions. Typical DSC data from a sample of $C_6H_6:C_6F_6$ is shown in Fig. 2, with further data on the components shown in Fig. S5.‡

The structures of the four phases solved from a mixture of powder and single-crystal diffraction methods are shown in

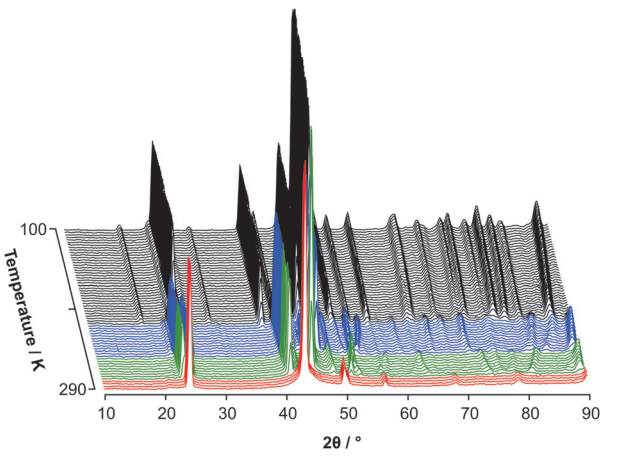

Fig. 1 Powder neutron diffraction data measured on the high-flux diffractometer D1B at the ILL, Grenoble, measured on heating a sample previously ground in liquid N_2 from 10 K to 290 K. Four solid state phases are clearly seen: phase I (red), phase II (green), phase III (blue) and phase IV (black).

Table 1 Lattice parameters for the four phases of $C_6D_6:C_6F_6$ measured on the same sample are obtained from data displayed in Fig. S4 and are based on a nominal neutron wavelength λ = 2.997 Å

$C_6H_6:C_6F_6$	Phase I	Phase II	Phase III	Phase IV
T/K	285	260	225	1.5
Space group	$R\bar{3}m$	$I2/m$	$P\bar{1}$	$P2_1/a$
a/Å	12.0088(5)	6.6044(6)	6.4012(3)	9.5163(3)
b/Å	12.0088(5)	12.3527(14)	12.3611(8)	7.4400(2)
c/Å	7.2521(5)	7.3190(4)	7.3137(2)	7.54278(17)
α/°	90	90	93.970(4)	90
β/°	90	99.257(6)	96.899(3)	95.6320(18)
γ/°	120	90	91.742(5)	90
V/Z/Å^3	301.91(6)	294.66(5)	286.35(3)	265.731(14)

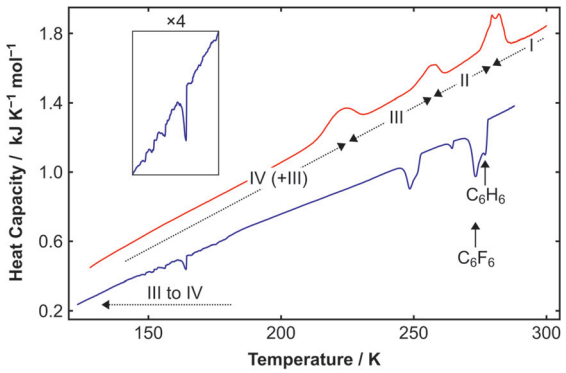

Fig. 2 DSC data obtained on cooling (blue curve) and heating (red curve) for $C_6H_6:C_6F_6$. Three solid state phase transitions and a freezing/melting transition are observed on cooling/heating. The transitions indicated by vertical arrows correspond to the freezing and melting transitions, respectively, of free or un-complexed benzene and hexafluorobenzene, which implies a phase equilibrium between the free molecules and the adduct in the solid sample. The features seen on cooling close to 150 K (and in the expanded insert) are reproducible in form but not in detail (that is, these features depend upon individual crystals of phase III changing to phase IV at different rates). In addition, they are only reproducible in form on cooling a sample from phase I suggesting that the thermal history of the sample influences the onset of the lowest temperature phase transition. This phase transition has been observed to display a large hysteresis, a hysteresis also indicated by the co-existence of phases III and IV seen in Fig. 1 and ESI‡ Fig. S3.

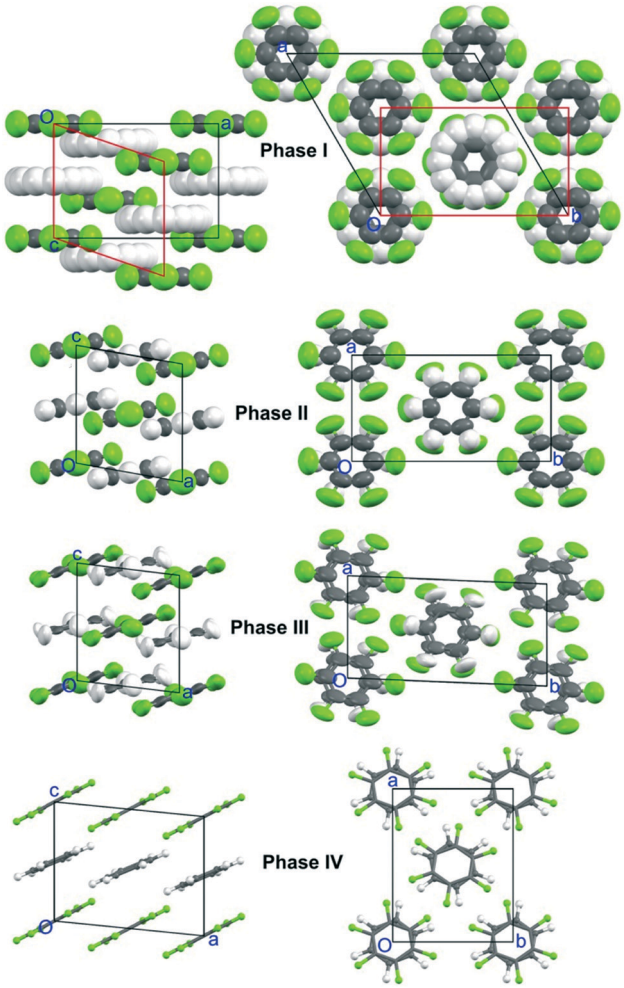

Fig. 3 Views of the crystal structures of phases IV to I of $C_6H_6:C_6F_6$ showing the evolution of the thermal motion as a function of temperature (the structures of the phases refer to temperatures: 1.5, 225, 260, and 280 K, respectively). Thermal ellipsoids are drawn at 50% probability. For the rhombohedral phase I, an equivalent body-centred monoclinic cell can be chosen (shown in red) that relates directly to the monoclinic cell of phase II. Phase III is a triclinic distortion of phase II, but its transition to phase IV involves a significant increase in the C–F···H–C bond dipole–bond dipole interactions between close packed columns of molecules. The crystallographic labelling of the atoms in each phase is shown in ESI‡ Fig. S7.

Fig. 3. Of these phases, phase IV was published previously,[9] and the structures of the other three phases are reported here having been solved from a mixture of powder and single-crystal diffraction studies (see ESI‡ Sect. 2 and 4). What is readily observed in Fig. 3 (and in detail in Fig. S9 and S10‡), is the interpenetration of the C–H and C–F bonds of molecules in neighbouring columns of the lowest temperature phase (IV). In this phase, the bonds on one type of molecule closely approach neighbouring molecules of the other type. Thus, C–H bonds in a C_6H_6 molecule are directed towards, and come very close to, F atoms of the C–F bonds of a C_6F_6 molecule in the layers above and below in adjacent columns (Fig. S10‡). Within a column, the C–H bonds on a C_6H_6 molecule are seen partially staggered with respect to the C–F bonds on the C_6F_6 molecules on either side of the C_6H_6 molecule by about 18° (Fig. 3). It is possible, therefore, to envisage a network of weakly-polarized hydrogen bond-like links between the closely packed columns as the means of stabilizing the solid lattice.

It is through the intermeshing network of C–H and C–F bonds (*i.e.* through a network of C–H···F–C interactions) originating in the different columns that the crystal architecture is stabilized. This lowest temperature phase of the solid adduct is like a molecular 'gear-box' with interlocking cogs (the interpenetrating C–H and C–F bonds) on closely-packed parallel shafts (or columns of molecules). The phase transition at 218 K is like a molecular clutch being engaged in a transmission system to change gear; in the solid, the molecular clutch leads to an increase in the inter-column spacing. The columns have separated, thus facilitating molecular motion of increasing amplitude, *e.g.* jump rotations of the C_6H_6

molecules around the six-fold axis of the molecule. This thermally driven motion continues for both C_6H_6 and C_6F_6 molecules right up to the melting point of the binary-adduct at 25 °C as shown by a study of the temperature dependence of the high-resolution laser Raman spectrum of this adduct.[27]

The change of geometry from staggered to eclipsed observed at the IV to III phase transition will modify the magnitude of the bond dipole–bond dipole interaction between the C–H and C–F bonds between columns. The separation of the parallel columns in the binary-adduct upon going from phase IV to phase III may be seen by examining the average separation of the bond dipoles of 2.61(7) Å in phase IV (from the 10 H···F distances seen in Fig. S9‡), and this same average (but over only 7 H···F distances seen in Fig. S15‡) which has become 2.71(8) Å in phase III. The columns have separated, and the attractive electrostatic potential between them has fallen.

In Fig. 4, the temperature dependence of the volume of the unit cell of the binary adduct derived from the original powder neutron diffraction data is presented. The largest percentage changes over this temperature range for the unit cell parameters are with respect to the *a*-axis (see ESI‡ Table S4 and Fig. S2). As the sample transforms from phase IV to phase I, the angle between the plane of the C_6F_6 molecule and the column axis changes dramatically as the molecules pivot about their centre-of-mass: 62.4° (IV), 71.5° (III), 75.8° (II), and 90° (I), as seen in Fig. 3, thus necessitating an increase in the lattice parameter *a*. Similar tilting behaviour is seen in the phases transitions of *s*-triazine,[28] which exhibits an analogous structural behaviour to $C_6H_6:C_6F_6$. Another

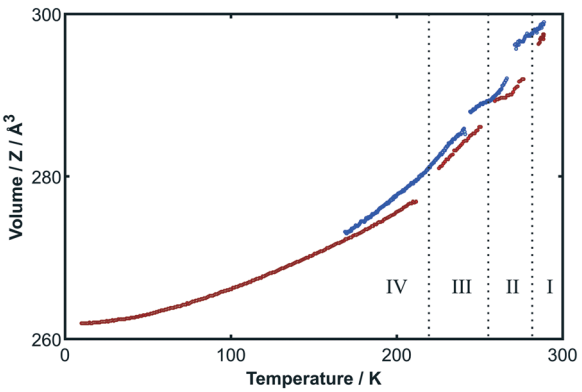

Fig. 4 Volume of the adduct pair $C_6D_6:C_6F_6$ as a function of heating (red) and cooling (blue) as derived from fitting 590 of the data sets shown in Fig. 1. Transition temperatures from the initial heating run on the ground sample are represented by the dotted vertical lines (IV–III at 218 K, III–II at 255 K, II–I at 281.5 K). Lattice parameters were obtained for phases II, III, and IV by Rietveld refinement with the structure of each phase constrained to that obtained from high-resolution powder diffraction data (phases III and IV) or single-crystal data (phase II). For phase I, lattice parameters were obtained by the LeBail method of whole pattern fitting but with the unit cell halved along *c* as C_6D_6 and C_6F_6 scatter almost equivalently. The error bars on the individual measurements are smaller than the size of the character used to indicate the value of the measurement. Further details are provided in the ESI.‡ The variation of individual unit-cell parameters with temperature is given in Table S4 and shown in Fig. S2.‡

consequence of the pivoting of the molecules is that the cell angle β increases with increasing temperature: 95.6° (IV), 96.7° (III), 100.1° (II), and 109.2° (I, for the monoclinic equivalent cell shown in red in Fig. 3). The *b*- and *c*-axes are found to not increase greatly, but just to a level as seen in molecular crystals.

The sequence of transitions on cooling involves the symmetry of the crystals changing from $R\bar{3}m$ to $I2/m$ to $P\bar{1}$ and finally to $P2_1/a$. The transitions from I to II and II to III involve displacive transitions with a simple super/sub-group symmetry relationship, in contrast to the transition III to IV which is unusual in that the lower temperature phase IV exhibits a higher symmetry than phase III. Despite the displacive transition, crystals do not form merohedral twins on cooling but shatter. This can be attributed to the large volume change at the transitions seen in Fig. 4.

Fig. 4 clearly demonstrates the hysteresis to be seen in the material. The hysteresis shows how phases III and IV can coexist over an extended range of temperature, and that the phase transition between phases III and IV is driven by the volume change, *i.e.* by the change of the C–H···F–C interactions between the columns. The volume change displayed in Fig. 4 is 14.2%, with the biggest increase at the highest temperatures, and at the phase transitions (indicated in the figure), consistent with the formation of a plastic phase (phase I) as also seen in the powder diffraction data (ESI‡ Fig. S4). For comparison, the volume of the unit cell of 1,3,5-$C_6H_3Me_3:C_6F_6$ increases by 8.7% over the range 90 to 300 K but there is no evidence for the formation of a plastic phase despite disorder of the methyl groups at elevated temperatures.[11] The plastic phase in $C_6H_6:C_6F_6$ with extensive disorder permits recrystallization of a powdered sample. Consequently, measurements on powdered samples will be dependent on the thermal history of the sample and the macroscopic structure of the material can be engineered by cycling the temperature. Phase II shows strong anisotropic behaviour. As the crystal structure evolves on heating towards the close packed columns that characterise phase I, in phase II the *a* axis expands rapidly to allow the plane of the rings to tilt (with the normal to the rings becoming more aligned along *c*) and the *b* axis contracts slightly (ESI‡ Fig. S2). By contrast, expansion is isotropic in the plastic phase I.

One of the many intriguing properties of this prototype, binary-adduct, $C_6H_6:C_6F_6$ is the increasingly-narrow temperature ranges of the four solid phases, which is clearly seen in Fig. 1 and 4. This behaviour may be explained by considering the close-packed columns of parallel, alternating benzene and hexafluorobenzene molecules as being held together by intermolecular electrostatic forces varying as r^{-3} (bond dipole moment–bond dipole moment interactions) and r^{-4} (molecular quadrupole moment–bond dipole moment interactions), where r is the spacing between the polar moieties in neighbouring columns. Fig. 4 and ESI‡ Fig. S2 show how rapidly the close-packed columns separate as the sample temperature increases, and as the attractive forces holding the columns together are falling as r^{-3} and r^{-4}, the higher temperature

phases of this material are increasingly short-lived for a constant rate of increase in temperature. There is an accelerated loss of cohesion between the columns. This explanation adds weight to the conjecture that it is possible to interpret the temperature-dependent dynamics and attractive intermolecular forces between the molecules in these binary-adducts in terms of simple models of intermolecular electrostatics involving localized and distributed interacting multipole moments.

Modern calculations on crystal structure predictions of the organic solid state are, as yet, unable to predict thermal motion with confidence, and so it is not possible to identify subtle phase transitions.[29] There is a delicate balance between intermolecular forces and thermal motion which determines the presence of any phase transition.

Experimental

Samples were prepared by mixing the components in a 1 : 1 molar ratio. DSC measurements were made using a liquid N_2 cooled PerkinElmer DSC8000 with a base temperature of 93 K. Variable temperature laboratory PXRD measurements were made using a Stoe Stadi-P diffractometer. SXD data sets were obtained on an Agilent SuperNova diffractometer. Neutron diffraction measurements were made using the powder diffractometers D1B and D1A at the ILL, Grenoble. Synchrotron X-ray measurements were made using beamline 2.3 at the SRS, Daresbury. Further details of all experiments are available in the ESI.‡

Conclusions

We have rationalized the structure of the four phases of benzene : hexafluorobenzene and are able to show how one form morphs into the next phase on heating/cooling in this prototypical material. The measurements presented here will be of interest to all those studying carbon–fluorine carbon–hydrogen interactions. Perhaps the main conclusion drawn from these extensive experimental observations is that it is possible to use relatively simple arguments about intermolecular electrostatics to assist in rationalising the observed crystal structures as a function of temperature. The model potentials (based on the interaction of bond dipole and quadrupole moments) are described in detail by Buckingham.[30] A future paper is planned in which these electrostatic interactions will be investigated with regard to the values of the enthalpy measurements given in the ESI.‡

Conflicts of interest

There are no conflicts to declare.

Acknowledgements

We acknowledge financial support from the EPSRC for funding the X-ray diffractometers (grant reference EP/K03930X/1). We thank Prof. Christoph Salzmann for use of the Royal Society funded DSC calorimeter and Isabella Fleminger for help with preliminary PXRD measurements. The attentive reader will have noticed that the results given here are based on two sets of data measured at an interval of more than a quarter century. Consequently, we thank the ILL for having put in a place a policy in the 1970s of permanently archiving all neutron data. The importance of data archives (in accordance with current UK Research Council policy and best practice) has been commented upon recently.[31] However, we note that retrieving data of this age is not as easy as one might wish. We are particularly grateful therefore to Dr Ronen E. Ghosh for his help in retrieving old data from the ILL archive.

References

1 J. D. Dunitz and A. Gavezzotti, *Chem. Soc. Rev.*, 2009, **38**, 2622–2633.
2 G. R. Desiraju, *J. Am. Chem. Soc.*, 2013, **135**, 9952–9967.
3 P. Panini and D. Chopra, in *Hydrogen Bonded Supramolecular Structures*, Lecture Notes in Chemistry, ed. Z. Li and L. Wu, Springer-Verlag, 2015, ch. 2, vol. 87, pp. 37–67.
4 A. Gavezzotti and L. L. Presti, *Cryst. Growth Des.*, 2016, **16**, 2952–2962.
5 J. A. K. Howard, V. J. Hoy, D. O'Hagan and G. T. Smith, *Tetrahedron*, 1996, **52**, 12613–12622.
6 V. R. Thalladi, H.-C. Weiss, D. Bläser, R. Boese, A. Nangia and G. R. Desiraju, *J. Am. Chem. Soc.*, 1998, **120**, 8702–8710.
7 K. Müller, C. Faeh and F. Diederich, *Science*, 2007, **317**, 1881–1886.
8 C. R. Patrick and G. S. Prosser, *Nature*, 1960, **187**, 1021.
9 J. H. Williams, J. K. Cockcroft and A. N. Fitch, *Angew. Chem., Int. Ed. Engl.*, 1992, **31**, 1655–1657.
10 T. Dahl, *Acta Chem. Scand.*, 1971, **25**, 1031–1039.
11 J. K. Cockcroft, R. E. Ghosh, J. J. Shephard, A. Singh and J. H. Williams, *CrystEngComm*, 2017, **19**, 1019.
12 T. Dahl, *Acta Chem. Scand.*, 1972, **26**, 1569–1575.
13 T. Dahl, *Acta Chem. Scand.*, 1973, **27**, 995–1003.
14 T. Dahl, *Acta Chem. Scand., Ser. A*, 1975, **29**, 170–174.
15 T. Dahl, *Acta Chem. Scand., Ser. A*, 1975, **29**, 699–705.
16 S. Bhandary and D. Chopra, *Cryst. Growth Des.*, 2018, **18**, 3027–3036.
17 D. F. R. Gilson and C. A. McDowell, *Can. J. Chem.*, 1966, **44**, 945–952.
18 T. Dahl, *Acta Chem. Scand., Ser. A*, 1988, **42**, 1–7.
19 J. H. Williams, *Acc. Chem. Res.*, 1993, **26**, 593–598.
20 J. H. Williams, *Mol. Phys.*, 1991, **73**, 99–112.
21 J. H. Williams, *Chem. Phys.*, 1993, **172**, 171–186.
22 N. M. D. Brown and F. L. Swinton, *J. Chem. Soc., Chem. Commun.*, 1974, 770–771.
23 J. Hernandez-Trujillo, M. Costas and A. Vela, *J. Chem. Soc., Faraday Trans.*, 1993, **89**, 2441–2443.
24 A. D. Buckingham, *J. Chem. Phys.*, 1959, **30**, 1580–1585.
25 M. R. Battaglia, A. D. Buckingham and J. H. Williams, *Chem. Phys. Lett.*, 1981, **78**, 421–423.

26 S. T. Bramwell and J. H. Williams, *J. Chem. Soc., Faraday Trans.*, 1992, **88**, 2721–2724.
27 J. H. Williams and M. Becucci, *Chem. Phys.*, 1993, **177**, 191–202.
28 J. H. Smith and A. I. M. Rae, *J. Phys. C: Solid State Phys.*, 1978, **11**, 1761–1770.
29 G. M. Day and C. H. Görbitz, *Acta Crystallogr., Sect. B: Struct. Sci., Cryst. Eng. Mater.*, 2016, **72**, 435–436.
30 A. D. Buckingham, *Adv. Chem. Phys.*, 1967, **13**, 107–142, (sect. V part D).
31 J. R. Helliwell, B. McMahon, J. M. Gussc and L. M. J. Kroon-Batenburg, *IUCrJ*, 2017, **4**, 714–722.